

Motion and Region Aware Adversarial Learning for Fall Detection with Thermal Imaging

Vineet Mehta*

Abhinav Dhall[†]*

Sujata Pal*

Shehroz Khan⁺

*Indian Institute of Technology Ropar, India

[†]Monash University, Australia

⁺KITE – Toronto Rehabilitation Institute, Canada

Abstract—Automatic fall detection is a vital technology for ensuring health and safety of people. Home based camera systems for fall detection often put people’s privacy at risk. Thermal cameras can partially/fully obfuscate facial features, thus preserving the privacy of a person. Another challenge is the less occurrence of falls in comparison to normal activities of daily living. As fall occurs rarely, it is non-trivial to learn algorithms due to class imbalance. To handle these problems, we formulate fall detection as an anomaly detection within an adversarial framework using thermal imaging camera. We present a novel adversarial network that comprise of two channel 3D convolutional auto encoders; one each handling video sequences and optical flow, which then reconstruct the thermal data and the optical flow input sequences. We introduce a differential constraint, a technique to track the region of interest and a joint discriminator to compute the reconstruction error. Larger reconstruction error indicates the occurrence of fall in a video sequence. The experiments on a publicly available thermal fall dataset show the superior results obtained in comparison to standard baseline.

Index Terms—Fall detection, adversarial learning, thermal camera, optical flow

I. INTRODUCTION

Automatic detection of fall is important due to the possibility of severe injury, high cost to the health system and psychological effect of a fall. However, due to their rarity of occurrence, traditional supervised machine learning classifiers are ill-posed for this problem [1]. There are also challenges in terms of collecting falls data as it can put people’s life in danger, whereas normal activities are easy to collect [1]. Therefore, in many realistic settings, there may be very few or no falls data available during training. Due to these skewed data situations, we adopted the fall detection as an anomaly detection problem [2]. In this setting, a classifier is trained on only abundantly available normal activities, during testing both normal and falls samples are presented to the classifier. Another challenge in video-based fall detection is to preserve the privacy of the person, which traditional RGB cameras cannot provide [3]. Thus, detecting falls in videos without explicitly knowing a persons identity is important from the real world usability of such systems. Thermal camera can partially or fully obfuscate a person’s identity and has been used in other fall detection applications [2]–[4].

The adversarial learning framework presents a unique opportunity to train a network to not only mimic the normal activities through a generator but also helps to discriminate it from the abnormal events through discriminator ([5], [6]). For video-based anomaly detection, normally, the generator is some variant of autoencoder, and the discriminator is a

feed-forward neural network, both of which are trained in an adversarial manner. The most successful previous works have mostly focused on learning spatio-temporal features by using 3D Convolutional Autoencoders (3DCAE) and 3D Convolution Neural Network (3DCNN) [6].

Performance of video-based fall detection may be marred by differences in background. This may become more prominent in thermal cameras where the intensities may change due to differences in heat (e.g. when person enters the scene). Therefore, it is important to focus on the region around the person. The relative motion of the person and objects around it can also provide useful information to detect falls. Region and motion based methods ([7], [8]) have shown superior performance in action recognition tasks. Therefore, we hypothesize that the learning spatio-temporal features utilizing region and motion awareness in video sequences would improve the detection of falls, when they are trained in an adversarial manner. To this end, we propose an adversarial learning framework that consists of two separate adversarial channels, with each arm having a thermal video sequence input (with extracted region of interest) and an optical flow input. Then, both the networks are trained jointly and their outputs are combined to give a score. Since both the adversarial networks are jointly trained, we expect to learn both motion and region based discriminatory features. The generator and discriminator in both the channels of the network are 3DCAE and 3DCNN.

II. RELATED WORK

There is scarce literature on detecting falls in videos in and adversarial manner with thermal cameras. We will now review studies that closely match with our work.

Fall Detection: With the camera sensors becoming advanced and economical, there are several interesting works [9]–[11], which use RGB cameras for data capturing. One major limitation of RGB sensors is the lack of privacy as the identity of the subject is not preserved. To overcome this limitation Vadivelu et al. [3] were one of the first fall detection works on thermal data. Further, Khan et al. [12] proposed using the thermal cameras in deep learning framework. Motivated by these work, we also use the thermal camera modality data in our experiments. The readers are also pointed to recent surveys [1], [13] in fall detection for more insights into different techniques proposed in the literature.

Anomaly Detection: Given the nature of fall events, which are rare, we follow the interesting works in abnormal activity detection. Chalapathy et al. [14] present a detailed survey on deep learning techniques for abnormal activity detection. Ribeiro et al. [15] proposed a CAE based technique for anomaly detection in videos. In an interesting work, Ravanbaksh et al. [16] proposed a video to flow and vice-versa generation adversarial approach for abnormal activity detection. Khan et al. [12] proposed the use of 3D CAE for abnormal activity detection applied to fall detection. They experimented on the Thermal Simulated Fall (TSF) dataset [3]. Fall being a spatio-temporal change in a subject’s pose, a limitation of the work is that the motion information is not explicitly added into the network. We build upon the adversarial learning work of Khan et al. [6] and propose a two channel network, with one channel explicitly learning the motion in the form of the optical flow. We also realise that there are may be empty frames in video sequences, where a person may not appear in the scene. Earlier works do not consider the absence or presence of person in the frame, which is important from the perspective of reducing the false positives due to high reconstruction error for background only. Motivated by these works, we further discuss the 3DCAE based framework below.

III. METHODS

Our proposed framework consists of two channels of adversarial learning. The input to first channel is the thermal video sequences and to the second channel is optical flow computed from the thermal video. Each channel of the adversarial framework consists of (i) training a 3DCAE to reconstruct the input sequence of frames and, (ii) a 3DCNN to discriminate them from the original sequences of frames. We trained this framework using only Activities of Daily Living (ADL) thermal frames and their corresponding optical flow frames, respectively. We extract Region of Interest from the thermal and the optical flow frames for region and motion based reconstruction. Combining these two adversarial network, we trained a joint network as shown in Figure 2 that provides the probability of a video sequence to be normal or a fall.

A. Advesarial Framework

1) *3DCAE-3DCNN*: Our spatio-temporal model consists of a 3DCAE and a 3D Discriminator (3DCNN). The architecture of the 3DCAE is similar to model proposed in [6]. We extend the same architecture for optical flow spatio-temporal model, which can be seen in Table I. We used 3D filters of 3×3 with a temporal depth of 5 in all layers of 3DCAE. The operations are same in the flow 3DCAE except for the second deconvolution layer which uses filter of 2×2 with temporal depth of 4, to reconstruct the temporal depth of odd length $T-I$.

The architecture of the 3DCNN is same as the encoder in 3DCAE, followed by a neuron at the end with a sigmoid function to output a probability of whether a sequence of frames are original or reconstructed. Batch normalization is used in all the layers of the 3D discriminator except for the

input layer. LeakyRelu activation is set in all hidden layers, with negative slope coefficient set to 0.2. ([6], [17]).

	Thermal 3DCAE	Flow 3DCAE
Input	(8, 64, 64, 1)	(7, 64, 64, 1)
Encoder	3D Conv - (8, 64, 64, 16)	3D Conv - (7, 64, 64, 16)
	3D Conv - (8, 32, 32, 8)	3D Conv - (7, 32, 32, 8)
	3D Conv - (4, 16, 16, 8)	3D Conv - (4, 16, 16, 8)
	3D Conv - (2, 8, 8, 8)	3D Conv - (2, 8, 8, 8)
Decoder	3D Deconv - (4, 16, 16, 8)	3D Deconv - (4, 16, 16, 8)
	3D Deconv - (8, 32, 32, 8)	3D Deconv - (7, 32, 32, 8)
	3D Deconv - (8, 64, 64, 16)	3D Deconv - (7, 64, 64, 16)
	3D Deconv - (8, 64, 64, 1)	3D Deconv - (7, 64, 64, 1)

TABLE I
CONFIGURATION OF THE 3DCAE.

2) *Adversarial Learning*: In this section, we first explain the general adversarial training as described in [6] which consists of 3DCAE (represented as \mathbf{R}), it takes the input sequence \mathbf{I} of window size T of normal ADL, and reconstructs the sequence, \mathbf{O} , which is then fed to fool 3DCNN (represented as \mathbf{D}). In our setting, \mathbf{R} maps \mathbf{I} to \mathbf{O} using the distribution of the target class p , i.e.

$$\mathbf{O} = \mathbf{I} \sim p$$

\mathbf{R} and \mathbf{D} are trained using standard GAN loss described as

$$L_{R+D} = E_{I \sim p}[\lg D(I)] + E_{O \sim p}[\lg(1 - D(O))] \quad (1)$$

We combine the adversarial loss with the MSE loss which is used only for Generator(\mathbf{R}). It is defined as

$$L_R = E[(I - O)^2] \quad (2)$$

The total loss function to minimize for \mathbf{R} is defined as:

$$L = L_{R+D} + \lambda L_R \quad (3)$$

where λ is a positive hyperparameter for weighted loss. The notations used for thermal and flow networks are $(\mathbf{I}_T, \mathbf{O}_T, \mathbf{R}_T, \mathbf{D}_T)$ and $(\mathbf{I}_F, \mathbf{O}_F, \mathbf{R}_F, \mathbf{D}_F)$, respectively.

B. ROI Extraction

The performance of video based fall detection can be severely impaired by the presence of artifacts present in the background. This situation can get worse with a thermal camera because changes in the heat can alter the background and overall intensity level of the frames in a video sequence [2]. Therefore, instead of focusing on reconstructing the entire background in a frame in a video sequence, a person is tracked and localised in the video frames using pre-trained object detection model and image processing techniques.

1) *Person Detection*: To the best of our knowledge, there are no pre-trained publicly available deep learning based models for person detection specifically in thermal images. To this end, we used the state-of-the-art R-FCN network [18] trained on COCO dataset [19]. As the TSF dataset contains only one subject in a frame, the bounding box with the highest confidence score is selected. There are no false proposals by the detector, however, the localized bounding box is found to fluctuate in size and position, which can degrade the tracking prediction.

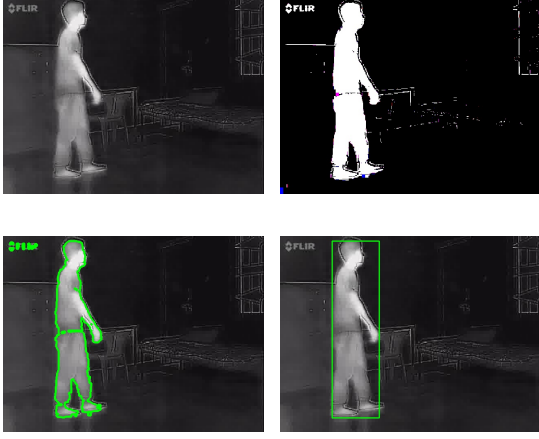


Fig. 1. Contour Box Localization (Section III-B).

2) *Contour Box Localization*: In thermal images, a person may appear brighter than the background due to differences in heat emitted by as a person and objects. Therefore, Otsu thresholding [20] is applied to the thermal image to separate dark background as shown in Fig. 1. The thresholded image may still contains background objects. We find the contours [21] on the thresholded image after applying morphological operations and select the biggest contour on the basis of inside area. The smallest box containing that contour blob is chosen as a candidate for person bounding box.

3) *Tracking*: We apply Kalman filtering on the the top-left and right-bottom coordinates of the bounding box with the constant velocity assumption. The tracker is initialised with the person detector and predicts the bounding box for the next frame and compared with the person detection bounding box (if detected) to check if the tracker drifts. In case of no detection, the age of tracker is increased, beyond that the tracker is stopped. Intersection of Union (IoU) is used in many tracking methods to match the bounding boxes; however, IoU is small when one box is large and other is small, which could be due to bad localization by the detector. Therefore, we also used other criteria such as ratio of area and checking for subset. At a particular instant, there could be at most three possible candidates for the person localization – Detect, Contour and Track box. Detect box confirms the presence of the person but it does not fit the person in most cases. Therefore, contour box and track box are used to improve the overall tracking. Algorithm 1 describes the summary.

4) *ROI Masking*: We remove the frames in which, person is not detected post tracking and rest of the frames are masked by their corresponding bounding box, which we call as ROI mask. For region based reconstruction, thermal 3DCAE is fed with the window of masked frames and a region based reconstruction loss L_{ROI} (instead of Eq. (3)) is defined as:

$$L_{ROI} = E_{ROI}[(ROI(I) - ROI(O))^2] \quad (4)$$

C. Motion Constraint and Reconstruction

Beside the appearance based constraint on R , the motion based constraint [22] and reconstruction would discriminate

Algorithm 1: Tracking Algorithm

```

Input : Frame
Output: FinalBox
DetectBox=Detector.GetLocalization(Frame);
if DetectBox is not None then
    ContourBox=GetBiggestContourBox(Frame);
    if Tracker is not None then
        TrackBox=Tracker.GetCurrentBox();
        if TrackBox matches with DetectBox then
            DetectBox=BoxSelection(DetectBox,TrackBox);
        else
            Tracker=None;
        end
    end
    if ContourBox matches with DetectBox then
        DetectBox=BoxSelection(DetectBox,ContourBox);
    end
    FinalBox=DetectBox;
    if Tracker is not None then
        Tracker.KalmanFilter(DetectBox);
        Tracker.Losses=0;
    else
        Tracker=InitializeTracker(DetectBox);
    end
end
else
    if Tracker is not None then
        TrackBox=Tracker.Predict();
        ContourBox=GetBiggestContourBox(Frame);
        if ContourBox matches with TrackBox then
            Tracker.Losses+=0.5;
            FinalBox=ContourBox;
            Tracker.KalmanFilter(ContourBox);
        else
            Tracker.CurrentBox=TrackBox;
            FinalBox=TrackBox;
            Tracker.Losses+=1;
        end
    end
end
if Tracker is not None and Tracker.Losses greater than
    MaxAge then
        Tracker=None;
        FinalBox=None;
end
Return FinalBox;

```

the unusual motion when a person falls.

1) *Difference Constraint*: In an interesting approach, Mathieu et al. [23] compute the difference and gradient based losses for future frame prediction. Inspired by them, for encoding local changes, we add an additional loss term in the thermal 3DCAE, which is based on MSE of difference frames of I

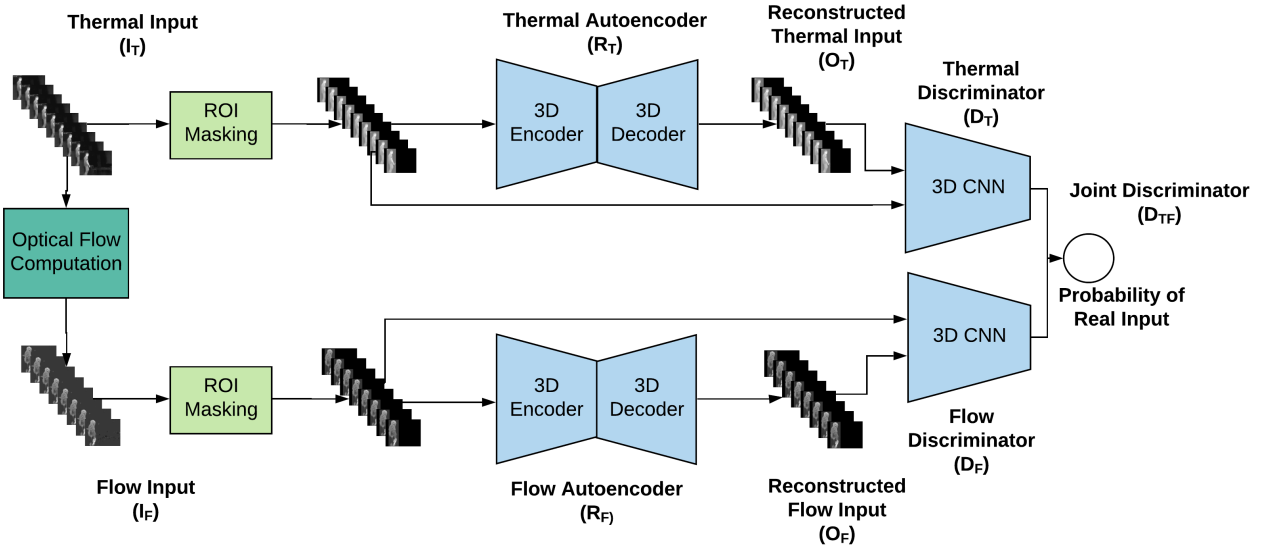


Fig. 2. The proposed fall detection network: the top and the bottom channels take thermal and flow data as input. The joint discriminator takes the outputs of the thermal and flow 3DCNN's as input.

and O . A difference frame is the residual map computed by subtracting two consecutive frames. We mask the difference frames by their respective ROI, which is the union of the ROIs of the two frames used to compute the difference frame. Further, the difference loss is defined as:

$$L_{Diff} = E_{ROI}[(DF(I) - DF(O))^2] \quad (5)$$

where $DF(X)$ represents the difference frames for the window X . Final loss for R in (3) with L_{ROI} and L_{Diff} is defined as:

$$L = L_{R+D} + \lambda_S L_{ROI} + \lambda_D L_{Diff} \quad (6)$$

where λ_S and λ_D are positive constants for weighted loss.

2) *Optical Flow Reconstruction*: Liu et al. [24] use constraint on the optical flow of the ground truth and reconstructed images for future frame prediction. They used CNN based model for flow estimation, which can facilitate backpropagation for optical flow loss but these models are trained on RGB images and may generate noise due to temperature changes in a thermal video. Therefore, we train a spatio-temporal adversarial network (R_F , D_F) for flow reconstruction which takes into input a window of optical flow frames. We compute the dense optical flow frames for two consecutive frames, according to [25]. We stack the flow in the x,y- direction and the magnitude to form a 3-dimensional image. [26]

To remove the noise due to temperature variations in optical flow images, we mask the flow images with their ROI. As defined earlier for difference frame, the ROI for flow image is the union of ROI of the two thermal frames used to compute the optical flow.

D. Thermal and Optical Flow Fusion

For thermal and flow based reconstruction, we propose a joint adversarial network which consists of two 3DCAE and a single discriminator. In the joint discriminator network D_{TF} , the individual 3DCNN networks - D_T and D_F are used where

the two individual discriminators to output probability are replaced by a single discriminator can be seen in Figure 2. For training, the joint loss function with ROI masking can be defined as:

$$L = L_{R+D} + \lambda_T L_{T_ROI} + \lambda_F L_{F_ROI} \quad (7)$$

where L_{T_ROI} and L_{F_ROI} are ROI based reconstruction loss for thermal and flow, respectively. The hyperparameters λ_T and λ_F are their corresponding positive constants for weighted loss. The joint loss function for ROI masking and difference constraint can be written as:-

$$L = L_{R+D} + \lambda_{T_S} L_{T_ROI} + \lambda_{T_D} L_{T_Diff} + \lambda_F L_{F_ROI} \quad (8)$$

where L_{T_Diff} and L_{T_ROI} are difference constraint and region based reconstruction loss defined earlier in (5) and (4).

IV. DETECTING UNSEEN FALLS

The strategy to detect unseen falls is shown in Figure 3 (derived from [2]). All the frames in the video, Fr_i , are broken down into windows of frames of length, $T = 8$, with stride=1. For the i^{th} window I_i , the 3DCAE outputs a reconstruction of this window, O_i . The reconstruction error ($R_{i,j}$) between the j^{th} frame of I_i and O_i can be calculated as (similar to Eq. (2))

$$R_{i,j} = E[(I_{i,j} - O_{i,j})^2] \quad (9)$$

where the expectation is taken over whole frame i.e $W \times H$. For the region based 3DCAE, it can be defined (similar to Eq. (4)) as follows:

$$R_{i,j} = E_{ROI}[(ROI(I_{i,j}) - ROI(O_{i,j}))^2] \quad (10)$$

where $ROI(I_{i,j})$ is the ROI of frame $I_{i,j}$ and the expectation is taken over ROI. There are two ways to detect unseen falls, (A) at the frame level, or (B) at the window level, which are described below.

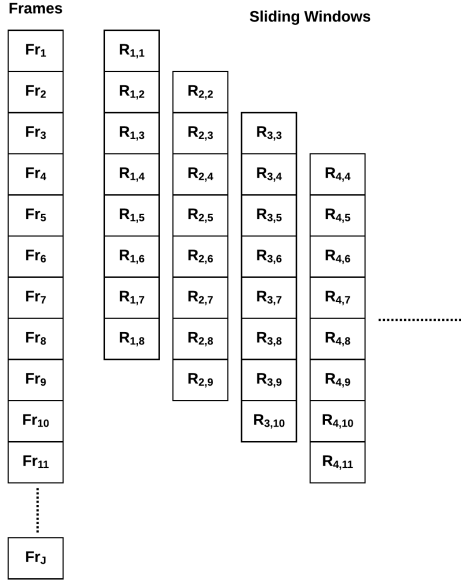


Fig. 3. Temporal sliding window showing error ($R_{i,j}$) per frame (Fr_j) with $T = 8$ (Section IV-B; Figure Source: [6]).

A. Frame Level Anomaly Score

In the frame level anomaly detection method, the reconstruction error ($R_{i,j}$) (obtained from the 3DCAE) is computed for every frame j^{th} across different windows. The average (C_{μ}^j) and standard deviation (C_{σ}^j) of a frame j across different windows are used as an anomaly score as follows [2]:

$$C_{\mu}^j = \begin{cases} \frac{1}{j} \sum_{i=1}^j R_{i,j} & j < T \\ \frac{1}{T} \sum_{i=1}^T R_{i,j} & j \geq T \end{cases} \quad (11)$$

$$C_{\sigma}^j = \begin{cases} \sqrt{\frac{1}{j} \sum_{i=1}^j (R_{i,j} - C_{\mu}^j)^2} & j < T \\ \sqrt{\frac{1}{T} \sum_{i=1}^T (R_{i,j} - C_{\mu}^j)^2} & j \geq T \end{cases}$$

B. Window Level Anomaly Score

In the window level anomaly detection method, we calculate the score for the entire window. For a particular window W_i of length T , the mean of reconstruction error of all the T frames (W_{μ}^j) and their standard deviation (W_{σ}^j) are used as an anomaly score, as follows [6]:

$$W_{\mu}^j = \frac{1}{T} \sum_{j=i}^{T+i-1} R_{i,j} \quad (12)$$

$$W_{\sigma}^j = \sqrt{\frac{1}{T} \sum_{j=i}^{T+i-1} (R_{i,j} - W_{\mu}^j)^2}$$

In difference constraint reconstruction models, the frame and window level anomaly score are calculated on the thermal input. Along with it, we calculate another window level anomaly score for a window by calculating the reconstruction error on difference frames (similar to Eq. (5)) and by taking the mean and standard deviation of reconstruction error over $T-1$ frames (similar to Eq. (12) with window length $T-1$).

In the optical flow reconstruction, we calculate the window level anomaly score from (12), where we take the window length to be $T-1$.

The number of fall frames required to present in a window (α) to set the ground-truth label of the entire window as fall, influence the detection of anomalies in window-based anomaly detection. We varied the value of α from 1 to T while testing to understand its impact.

V. EXPERIMENTS



Fig. 4. TSF dataset [3] samples with activity information. Here, top row shows empty room frames; middle row shows ADL frames-walking and lying on bed; Bottom row shows the fall while sitting in chair and fall during walking, respectively.

Dataset: We use the publicly available Thermal Simulated Fall dataset [3] containing 44 thermal videos with a spatial resolution of 640x480. There are 9 videos with normal ADL and 35 videos containing falls and other normal activities. The ADL frames include different scenarios such as an empty room, a person entering the room, sitting on the chair, or lying in bed, whereas the fall frames include a person falling from the chair, bed, or falling while walking. Some of the ADL and fall frames are shown in Fig. 4. ADL videos contain a total of 22,116 frames.

Data Processing: We perform person tracking on videos, when a person is not detected continuously for 10 frames, we break the video and create sub videos, resulting in 22 sub videos, which further contain 12,454 frames from ADL videos for training. For ROI computation, the threshold for region selection is empirically set to 0.3. We perform sliding window on videos with stride one to create windows of length $T=8$, which creates a total of 12,300 windows from ADL sub

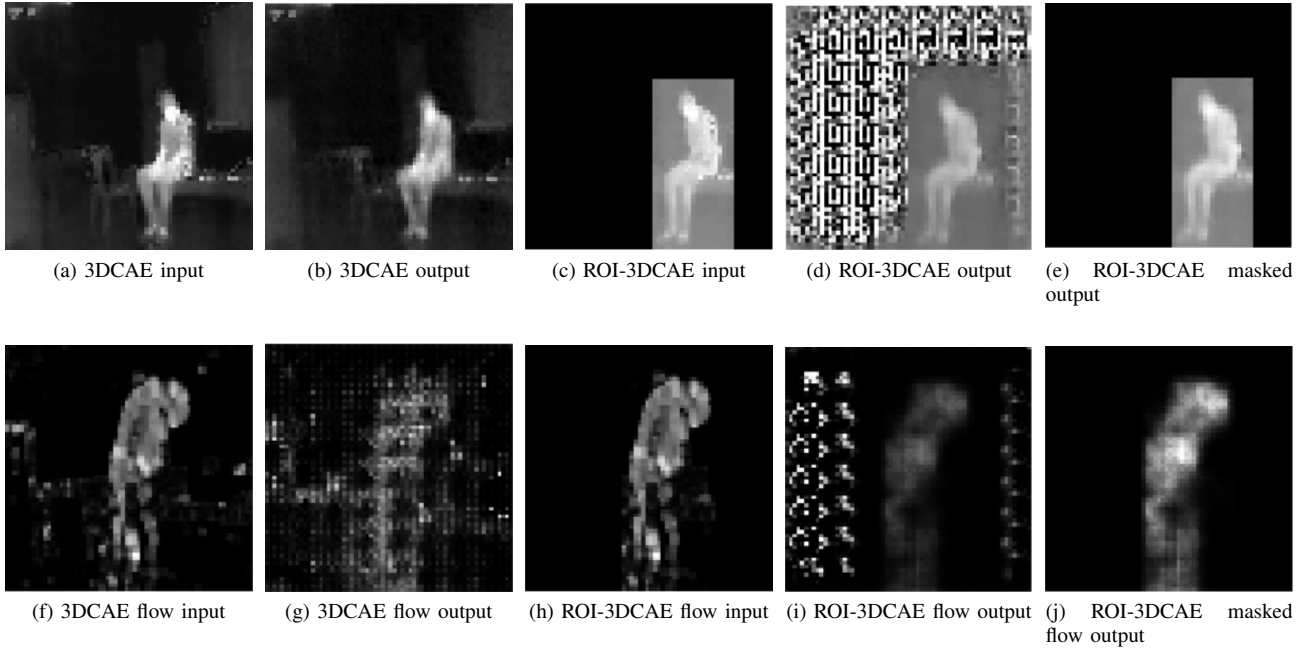


Fig. 5. Channel-wise qualitative results: the top row images [(a)-(e)] and bottom row images [(f)-(j)] are the inputs and corresponding outputs of the thermal data channel and flow magnitude channels, respectively.

videos. We normalize frame in the range $[-1, 1]$ by normalizing using mean pixel values [17] followed by resizing to 64×64 .

ROI processing: For region-based reconstruction in thermal images, we perform normalization on the pixels inside the ROI and then compute the masked frame by ROI masking, in which all the pixels outside the ROI are set to -1 . Finally, an ROI masked frame contains pixel value in the range $[-1, 1]$ inside the ROI and -1 outside the ROI.

Optical flow image pre-processing: Each channel of a flow image (x - y -magnitude) is rescaled in the range of $[-1, 1]$ by min-max normalization. For region-based reconstruction in flow images, we perform ROI masking as described earlier for the normalized thermal image, where the ROI of the optical flow frame is the union of the corresponding consecutive frames.

A. Network Implementations

We trained two spatio-temporal models - one which reconstructs the thermal window and other reconstructs the optical flow window, called **Thermal-3DCAE** and **Flow-3DCAE**, respectively.

For region based reconstruction, we trained two spatio-temporal models on thermal data, one with ROI masking and ROI loss (Eq. (4)) described earlier and the other one with the addition of difference constraint in the region construction named as **Thermal-ROI-3DCAE** and **Thermal-Diff-ROI-3DCAE**. We trained one spatio-temporal model for flow with region-based construction, named as **Flow-ROI-3DCAE**.

In the fusion model, we trained two models: one without the difference constraint (**Fusion-ROI-3DCAE**) and one with it (**Fusion-Diff-ROI-3DCAE**).

We used SGD optimizer with learning rate as 0.0002 for the 3DCNN discriminator and adadelta optimizer for the 3DCAE in all the spatio-temporal models. All the models are trained for 300 epochs. The hyperparameters (λ 's) used for the weighted loss (Eq-(3), (6) and (7)) are varied between three values [0.1, 1 and 10].

B. Evaluation Metrics

For anomaly detection problems, the Area Under Curve (AUC) of Receiver Operation Characteristic (ROC) is widely used as a performance metric. In fall detection, the data is highly imbalanced, and our focus is on the positive class i.e. fall. Therefore, we also plot the Precision-Recall (PR) curve and calculate its Area Under Curve (AUC).

As discussed earlier, we used two methods for calculating the reconstruction scores (mean and standard deviations) - frame and window. Moreover, we also defined window based anomaly scores on the difference constraint loss. We calculated AUC for ROC and PR based on all these scores.

C. Ablation Studies

1) **3DCAE:** In **Thermal-3DCAE**, the thermal window is input. The reconstruction output by **Thermal-3DCAE** can be seen in Figure 5. We also trained two different **Thermal-3DCAE** models by changing the thermal input- (1) resizing the input ROI to 64×64 and (2) ROI pooling. We observe that these models perform worse and the results for them are not reported. We argue that resizing the ROI leads to geometric distortions and introduces motion on the borders even if the subject is not moving.

Optical Flow: As described earlier, optical flow images contain noise due to temperature variation (in recording sensor

Method	Frame		Window																
			1		2		3		4		5		6		7		8		
Tolerance(α)	C_μ	C_σ	W_μ	W_σ	W_μ	W_σ	W_μ	W_σ	W_μ	W_σ	W_μ	W_σ	W_μ	W_σ	W_μ	W_σ	W_μ	W_σ	
3DCAE																			
Thermal	0.9	0.88	0.83	0.86	0.85	0.88	0.87	0.89	0.89	0.9	0.9	0.91	0.91	0.92	0.92	0.92	0.93	0.92	
Flow	ND	ND	0.75	0.73	0.76	0.74	0.78	0.75	0.79	0.77	0.8	0.78	0.81	0.79	0.82	0.79	0.83	0.8	
ROI 3DCAE																			
Thermal	0.92	0.89	0.85	0.87	0.87	0.89	0.89	0.9	0.91	0.91	0.92	0.92	0.93	0.93	0.94	0.93	0.95	0.94	
Flow	ND	ND	0.85	0.82	0.86	0.84	0.87	0.84	0.88	0.85	0.89	0.85	0.9	0.86	0.9	0.86	0.91	0.87	
Diff-ROI-3DCAE																			
Thermal-ROI score	0.92	0.9	0.86	0.89	0.88	0.9	0.9	0.91	0.91	0.92	0.93	0.93	0.94	0.94	0.95	0.94	0.96	0.94	
Thermal- Diff score	ND	ND	0.89	0.91	0.9	0.93	0.92	0.94	0.93	0.95	0.94	0.96	0.96	0.97	0.96	0.97	0.97	0.97	
Fusion-ROI-3DCAE																			
Thermal-ROI score	0.93	0.9	0.85	0.89	0.87	0.9	0.89	0.92	0.91	0.93	0.92	0.94	0.94	0.94	0.95	0.94	0.96	0.95	
Flow-ROI score	ND	ND	0.86	0.85	0.87	0.86	0.88	0.87	0.89	0.87	0.9	0.88	0.91	0.89	0.91	0.89	0.92	0.9	
Fusion-Diff-ROI-3DCAE																			
Thermal-ROI score	0.93	0.9	0.85	0.88	0.87	0.9	0.89	0.91	0.91	0.93	0.92	0.94	0.93	0.94	0.94	0.95	0.95	0.95	
Thermal- Diff score	ND	ND	0.89	0.91	0.9	0.93	0.92	0.94	0.93	0.95	0.95	0.96	0.96	0.97	0.96	0.97	0.97	0.97	
Flow-ROI score	ND	ND	0.85	0.84	0.86	0.85	0.87	0.86	0.88	0.86	0.89	0.87	0.9	0.88	0.9	0.88	0.91	0.88	

TABLE II

DIFFERENT NETWORK CONFIGURATION COMPARISON BASED ON AUC ROC FOR FRAME AND WINDOW LEVEL ANALYSIS.

Method	Frame		Window																
			1		2		3		4		5		6		7		8		
Tolerance(α)	C_μ	C_σ	W_μ	W_σ	W_μ	W_σ	W_μ	W_σ	W_μ	W_σ	W_μ	W_σ	W_μ	W_σ	W_μ	W_σ	W_μ	W_σ	
3DCAE																			
Thermal	0.48	0.47	0.48	0.51	0.49	0.52	0.51	0.52	0.52	0.53	0.54	0.53	0.55	0.53	0.56	0.51	0.56	0.47	
Flow	ND	ND	0.25	0.21	0.25	0.21	0.25	0.21	0.25	0.2	0.25	0.2	0.24	0.19	0.23	0.18	0.22	0.16	
ROI 3DCAE																			
Thermal	0.57	0.55	0.58	0.56	0.61	0.57	0.63	0.57	0.65	0.57	0.57	0.68	0.69	0.57	0.7	0.55	0.71	0.52	
Flow	ND	ND	0.44	0.34	0.45	0.35	0.45	0.34	0.45	0.33	0.46	0.31	0.46	0.3	0.45	0.28	0.44	0.25	
Diff-ROI-3DCAE																			
Thermal-ROI score	0.56	0.57	0.6	0.58	0.62	0.6	0.65	0.6	0.67	0.61	0.69	0.61	0.71	0.6	0.71	0.57	0.72	0.52	
Thermal- Diff score	ND	ND	0.62	0.67	0.64	0.7	0.67	0.71	0.69	0.72	0.72	0.74	0.74	0.74	0.74	0.73	0.76	0.7	
Fusion-ROI-3DCAE																			
Thermal-ROI score	0.58	0.56	0.59	0.59	0.61	0.6	0.63	0.61	0.66	0.61	0.68	0.61	0.7	0.6	0.7	0.57	0.71	0.53	
Flow-ROI score	ND	ND	0.46	0.4	0.47	0.4	0.48	0.39	0.48	0.38	0.48	0.37	0.49	0.37	0.48	0.35	0.45	0.32	
Fusion-Diff-ROI-3DCAE																			
Thermal-ROI score	0.57	0.57	0.59	0.58	0.62	0.59	0.64	0.6	0.66	0.6	0.69	0.6	0.71	0.59	0.71	0.57	0.72	0.54	
Thermal- Diff score	ND	ND	0.62	0.67	0.65	0.7	0.67	0.71	0.69	0.72	0.72	0.74	0.74	0.74	0.75	0.72	0.76	0.7	
Flow-ROI score	ND	ND	0.45	0.37	0.45	0.37	0.46	0.36	0.45	0.35	0.45	0.35	0.45	0.34	0.44	0.33	0.42	0.3	

TABLE III

DIFFERENT NETWORK CONFIGURATION COMPARISON BASED ON AUC PR FOR FRAME AND WINDOW LEVEL ANALYSIS.

used in the TSF dataset) due to which the reconstruction quality is also noisy (Figure 5(g)).

2) **ROI-3DCAE**: The output of **Thermal-ROI-3DCAE** and **Flow-ROI-3DCAE** can be seen in the Figure 5. We observe that the region based reconstruction improves the reconstruction quality in the ROI region and the model is able to understand which region is to reconstruct which can be seen in the images (c), (d) and (e) of Figure 5. The masked thermal ROI image(c) is given input to the model, the output(d) by the model reconstructs only the ROI region and we can compare the reconstruction quality after masking the output(e). Similar behaviour is observed for **Flow-ROI-3DCAE** which can be seen in the images (h), (i) and (j) of Figure 5.

3) **Diff-ROI-3DCAE**: To understand the impact of difference constraint, we compare the results of **Thermal-ROI-3DCAE** and diff score of **Thermal-ROI-Diff-3DCAE** which can be seen in Tables II and III (Row no.- 8 and 12). It can be seen that there is a great improvement in AUC ROC and PR calculated by window-based anomaly method. It suggests that

the difference constraint makes the model more discriminative.

4) **Fusion-3DCAE**: We compare the results of **Thermal-ROI-3DCAE** and **Flow-ROI-3DCAE** with Thermal-ROI score and Flow-ROI score of **Fusion-ROI-3DCAE** which can be seen in Tables II and III (Row no.-8,9,14 and 15). We observe that there is a small increment in the score of Thermal-3DCAE and a substantial increment in Flow-3DCAE, which indicates that joint learning improved the learning of flow reconstructor.

Fusion-Diff-ROI-3DCAE: We observed the same increase in window-based anomaly score without any decrease in reconstruction quality on the addition of difference constraint in the **Fusion-ROI-3DCAE** networks as observed between **Thermal-ROI-3DCAE** **Thermal-Diff-ROI-3DCAE**. It suggests that the difference constraint loss can be used in spatio-temporal models for temporal discriminative learning.

VI. RESULTS

The AUC ROC and AUC PR values for all the different networks is presented in Tables II and III. In each table, we

Method	ROC AUC	
	C_μ	C_σ
Conv-LSTM AE [6]	0.76	0.83
DSTCAE-C3D [2]	0.93	0.97
3DCAE-3DCNN [4]	0.95	0.95
Fusion-Diff-ROI-3DCAE (Ours)	0.93	0.90

TABLE IV
ROC AUC COMPARISON FOR FRAME BASED SCORES.

show AUC values for both frame and window based anomaly scores with the variation in tolerance(α)- the number of fall frames to label a window as fall. Each numerical value in the table represents the average AUC across all videos [2], [4], [6]. Results shown in Tables II and III can be summarized as

- 1) There is a great improvement in the AUC ROC and PR by region based construction which confirms the importance of region awareness.
- 2) The addition of difference constraint boosts the performance by significant amount which indicate its importance in the learning of spatio-temporal models.
- 3) The fusion models leads to increase in performance of the overall pipeline.

Comparison with existing methods: In the previous works, Conv-LSTM AE [4], DSTCAE-C3D [2] and spatio-temporal model similar to our method 3DCAE-3DCNN [6], ROC AUC values on frame based anomaly score is reported. The comparison can be seen in the Table IV. However, we can not directly compare the scores due to the following reasons:-

- 1) In the previous methods, empty room frames are also used while training and testing as the person tracking is not performed whereas we remove these frames as these are not required for fall detection. The consideration of these frames generates more quantitative numbers in the evaluation as the empty room frames are similar in both ADL and Fall frames.
- 2) In the previous methods, the input frames include the background, whereas our region-based models focus only on the region where the person is present as we focus on learning a generic model that can be used even when the background is changed.

VII. CONCLUSION

Fall detection is a non-trivial problem due to large imbalance in data; thus, we formulate it as an anomaly detection problem. In this problem, we trained the model on only normal ADL and predicts whether the test sample is normal ADL or a fall. Building upon the advantages of adversarial learning paradigm, we present a two channel adversarial learning framework to learn spatio-temporal features by extracting region of interest and its generated optical flow followed by a joint discriminator. This network predicts the fall probability, given an input sequence. We note that the introduction of ROI around the person and difference loss function help in better performance in fall event detection. The optical flow information is also useful in the network and the fused method performs better than the raw thermal analysis only.

REFERENCES

- [1] S. S. Khan and J. Hoey, "Review of fall detection techniques: A data availability perspective," *Medical engineering & physics*, vol. 39, pp. 12–22, 2017.
- [2] J. Nogas, S. S. Khan, and A. Mihailidis, "Deepfall: Non-invasive fall detection with deep spatio-temporal convolutional autoencoders," *Journal of Healthcare Informatics Research*, vol. 4, no. 1, pp. 50–70, 2020.
- [3] S. Vadivelu, S. Ganesan, O. R. Murthy, and A. Dhall, "Thermal imaging based elderly fall detection," in *ACCV*. Springer, 2016, pp. 541–553.
- [4] J. Nogas, S. S. Khan, and A. Mihailidis, "Fall detection from thermal camera using convolutional lstm autoencoder," in *Proceedings of the 2nd workshop on Aging, Rehabilitation and Independent Assisted Living, IJCAI Workshop*, 2018.
- [5] T. Schlegl, P. Seeböck, S. M. Waldstein, G. Langs, and U. Schmidt-Erfurth, "f-anogan: Fast unsupervised anomaly detection with generative adversarial networks," *Medical image analysis*, vol. 54, pp. 30–44, 2019.
- [6] S. S. Khan, J. Nogas, and A. Mihailidis, "Spatio-temporal adversarial learning for detecting unseen falls," *arXiv preprint arXiv:1905.07817*, 2019.
- [7] D. Li, Z. Qiu, Q. Dai, T. Yao, and T. Mei, "Recurrent tubelet proposal and recognition networks for action detection," in *ECCV*, September 2018.
- [8] J. Carreira and A. Zisserman, "Quo vadis, action recognition? a new model and the kinetics dataset," in *proceedings of the IEEE CVPR*, 2017, pp. 6299–6308.
- [9] G. Baldewijns, G. Debarde, G. Mertes, B. Vanrumste, and T. Croonenborghs, "Bridging the gap between real-life data and simulated data by providing a highly realistic fall dataset for evaluating camera-based fall detection algorithms," *Healthcare technology letters*, vol. 3, no. 1, pp. 6–11, 2016.
- [10] K. Sehairi, F. Chouireb, and J. Meunier, "Elderly fall detection system based on multiple shape features and motion analysis," in *2018 ISCV*. IEEE, 2018, pp. 1–8.
- [11] S. Ezatzadeh and M. R. Keyvanpour, "Vifa: an analytical framework for vision-based fall detection in a surveillance environment," *Multimedia Tools and Applications*, vol. 78, no. 18, pp. 25 515–25 537, 2019.
- [12] S. S. Khan, M. E. Karg, D. Kulić, and J. Hoey, "Detecting falls with x-factor hidden markov models," *Applied Soft Computing*, vol. 55, pp. 168–177, 2017.
- [13] L. Ren and Y. Peng, "Research of fall detection and fall prevention technologies: A systematic review," *IEEE Access*, vol. 7, pp. 77 702–77 722, 2019.
- [14] R. Chalapathy and S. Chawla, "Deep learning for anomaly detection: A survey," *arXiv preprint arXiv:1901.03407*, 2019.
- [15] M. Ribeiro, A. E. Lazzaretti, and H. S. Lopes, "A study of deep convolutional auto-encoders for anomaly detection in videos," *Pattern Recognition Letters*, vol. 105, pp. 13–22, 2018.
- [16] M. Ravanbakhsh, M. Nabi, E. Sangineto, L. Marcenaro, C. Regazzoni, and N. Sebe, "Abnormal event detection in videos using generative adversarial nets," in *2017 IEEE International Conference on Image Processing (ICIP)*. IEEE, 2017, pp. 1577–1581.
- [17] A. Radford, L. Metz, and S. Chintala, "Unsupervised representation learning with deep convolutional generative adversarial networks," *arXiv preprint arXiv:1511.06434*, 2015.
- [18] S. Ren, K. He, R. Girshick, and J. Sun, "Faster r-cnn: Towards real-time object detection with region proposal networks," in *Advances in neural information processing systems*, 2015, pp. 91–99.
- [19] T.-Y. Lin, M. Maire, S. Belongie, J. Hays, P. Perona, D. Ramanan, P. Dollár, and C. L. Zitnick, "Microsoft coco: Common objects in context," in *European conference on computer vision*. Springer, 2014, pp. 740–755.
- [20] N. Otsu, "A threshold selection method from gray-level histograms," *IEEE transactions on systems, man, and cybernetics*, vol. 9, no. 1, pp. 62–66, 1979.
- [21] S. Suzuki *et al.*, "Topological structural analysis of digitized binary images by border following," *Computer vision, graphics, and image processing*, vol. 30, no. 1, pp. 32–46, 1985.
- [22] T.-N. Nguyen and J. Meunier, "Anomaly detection in video sequence with appearance-motion correspondence," in *Proceedings of the IEEE International Conference on Computer Vision*, 2019, pp. 1273–1283.

- [23] M. Mathieu, C. Couprie, and Y. LeCun, "Deep multi-scale video prediction beyond mean square error," *arXiv preprint arXiv:1511.05440*, 2015.
- [24] W. Liu, W. Luo, D. Lian, and S. Gao, "Future frame prediction for anomaly detection—a new baseline," in *Proceedings of the IEEE Conference on CVPR*, 2018, pp. 6536–6545.
- [25] G. Farnebäck, "Two-frame motion estimation based on polynomial expansion," in *Scandinavian conference on Image analysis*. Springer, 2003, pp. 363–370.
- [26] G. Gkioxari and J. Malik, "Finding action tubes," in *The IEEE Conference on Computer Vision and Pattern Recognition (CVPR)*, June 2015.